Article

Cell Reports

Impaired LRP6-TCF7L2 Activity Enhances Smooth Muscle Cell Plasticity and Causes Coronary Artery Disease

Graphical Abstract

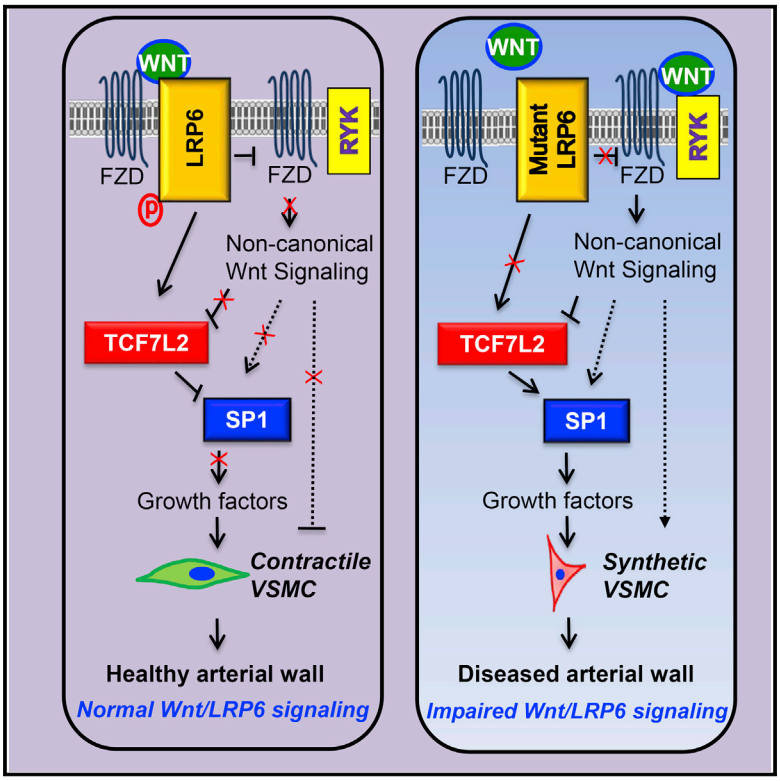

Authors

Roshni Srivastava, Jiasheng Zhang, Gwang-woong Go, Anand Narayanan, Timothy P. Nottoli, Arya Mani

Correspondence

arya.mani@yale.edu

In Brief

Srivastava et al. demonstrate that loss of LRP6 activity results in loss of vascular smooth muscle cell (VSMC) differentiation, neointima formation, and coronary artery disease (CAD) via reduced TCF7L2-dependent inhibition of Sp1. In vivo, Wnt3a activates LRP6 and rescues TCF7L2 expression and the vascular phenotype, signifying the important role of the Wnt/LRP6/TCF7L2 in maintaining vascular integrity.

Highlights

- *LRP6*^{R611C} mice exhibit aortic medial hyperplasia and coronary artery disease
- *LRP6*^{R611C} mice VSMCs have reduced TCF7L2 expression and are undifferentiated
- Activation of non-canonical Wnt is increased in *LRP6*^{R611C} mice VSMCs
- Wnt3a normalizes the non-canonical Wnt and TCF7L2 activities and rescues the phenotype

Srivastava et al., 2015, Cell Reports *13*, 746–759
October 27, 2015 ©2015 The Authors
http://dx.doi.org/10.1016/j.celrep.2015.09.028

OPEN ACCESS
CellPress

Cell Reports
Article

Impaired LRP6-TCF7L2 Activity Enhances Smooth Muscle Cell Plasticity and Causes Coronary Artery Disease

Roshni Srivastava,[1] Jiasheng Zhang,[1] Gwang-woong Go,[1,4] Anand Narayanan,[1] Timothy P. Nottoli,[2] and Arya Mani[1,3,*]
[1]Yale Cardiovascular Research Center, Department of Internal Medicine, Yale University School of Medicine, New Haven, CT 06520, USA
[2]Section of Comparative Medicine, Yale University School of Medicine, New Haven, CT 06520, USA
[3]Department of Genetics, Yale University School of Medicine, New Haven, CT 06520, USA
[4]Present address: Department of Food and Nutrition, Kookmin University, Seoul 02707, South Korea
*Correspondence: arya.mani@yale.edu
http://dx.doi.org/10.1016/j.celrep.2015.09.028

SUMMARY

Mutations in Wnt-signaling coreceptor *LRP6* have been linked to coronary artery disease (CAD) by unknown mechanisms. Here, we show that reduced LRP6 activity in *LRP6*^{R611C} mice promotes loss of vascular smooth muscle cell (VSMC) differentiation, leading to aortic medial hyperplasia. Carotid injury augmented these effects and led to partial to total vascular obstruction. *LRP6*^{R611C} mice on high-fat diet displayed dramatic obstructive CAD and exhibited an accelerated atherosclerotic burden on LDLR knockout background. Mechanistically, impaired LRP6 activity leads to enhanced non-canonical Wnt signaling, culminating in diminished TCF7L2 and increased Sp1-dependent activation of PDGF signaling. Wnt3a administration to *LRP6*^{R611C} mice improved LRP6 activity, led to TCF7L2-dependent VSMC differentiation, and rescued post-carotid-injury neointima formation. These findings demonstrate the critical role of intact Wnt signaling in the vessel wall, establish a causal link between impaired LRP6/TCF7L2 activities and arterial disease, and identify Wnt signaling as a therapeutic target against CAD.

INTRODUCTION

Aberrant Wnt signaling is implicated in pathogenesis of coronary artery disease and its metabolic risk factors. Rare, highly penetrant mutations with large effects in the Wnt-signaling coreceptor *LRP6* (low-density lipoprotein-receptor-related protein 6) gene have been associated with autosomal dominant early onset CAD (OMIM: ADCADII; Go et al., 2014; Mani et al., 2007; Singh et al., 2013b; Wang et al., 2012; Xu et al., 2014). The canonical Wnt-signaling pathway consists of a cascade of events that initiate after binding of a Wnt protein ligand to a Frizzled family receptor and phosphorylation of its coreceptors LRP5/6. This leads to stabilization of β-catenin and its translocation to the nucleus, where it interacts with TCF/LEF family transcriptional activators to promote gene expression that regulates cell cycle, cell growth, and proliferation. Wnt proteins also activate different β-catenin-independent signaling pathways that are collectively referred to as non-canonical Wnt signaling. This pathway involves activation of CAMKII, JNK, Rho, Rac, and ROCK. Recent studies suggest that canonical and non-canonical pathways reciprocally inhibit each other and exert opposing effects on common targets such as TCF7L2.

CAD is an extremely heterogeneous disorder with various etiologies. Whereas arterial occlusive disease is generally attributed to lipid- and macrophage-rich atherosclerotic plaques, several lines of evidence implicate VSMC proliferation as a key event in CAD development (Ross and Glomset, 1973). Coronary and carotid artery occlusions in patients with autosomal dominant mutations in the smooth muscle alpha actin gene (SM α-actin, a.k.a., ACTA2) have been linked to excessive proliferation of VSMC (Milewicz et al., 2010). Pathological studies in young subjects with death from myocardial infarction without a plaque rupture have revealed excessive VSMC proliferation and endothelial erosion in absence of overt inflammation (Virmani et al., 2000). In addition, recent data have implicated smooth muscle cell transdifferentiation in atherogenesis. New studies in human atherosclerotic lesions have shown that about 50% of foam cells and 40% of CD-68-positive cells are of VSMC origin (Allahverdian et al., 2014). Fate mapping in apolipoprotein-E-deficient mice has shown that VSMCs deficient for SMC markers undergo transformation into macrophage-like cells and account for major part of advanced atherosclerotic lesions (Feil et al., 2014). Finally, lineage tracing of SMC in Apoe−/− mice has shown that large number of macrophages and mesenchymal stem cells (MSCs) in advanced atherosclerotic lesions are SMC-derived (Shankman et al., 2015). These findings provide strong evidence for the critical role of VSMCs in CAD development.

Various indirect evidence has implicated Wnt signaling in regulation of VSMC plasticity (Mill and George, 2012). However, absence of an animal model has prohibited in-depth investigation into the role of Wnt signaling in regulation of VSMC plasticity in the context of CAD development. By introducing the human *LRP6*^{R611C} mutation into the endogenous mouse *LRP6* gene,

we have generated one of the few existing mouse models of CAD. Here, we describe the mechanisms by which an impaired Wnt/LRP6/TCF7L2 axis alters VSMC phenotype, causes CAD, and promotes atherosclerosis.

RESULTS

LRP6^{R611C} Mice on Chow Diet Develop Aortic Medial Hyperplasia

The rare *LRP6*^{R611C} mutation found in humans causes severe early onset coronary artery disease. To understand the role of *LRP6* in cardiovascular disease, we generated a knockin mouse expressing this mutant in the endogenous *LRP6* locus. VSMCs cultured from mice homozygous for *LRP6*^{R611C} mutation (from now on referred to as *LRP6*^{R611C} mice) exhibited reduced LRP6 activity measured by LRP6 phosphorylation levels and resulted in impaired canonical Wnt-signaling activity, manifested by reduced expression of its downstream target cyclin D1 mRNA (Figures 1A and 1B). The effect of *LRP6* mutation on the aortic wall was assessed in 3- to 6-month-old *LRP6*^{R611C} mice on chow diet and compared with age- and gender-matched wild-type mice. *LRP6*^{R611C} aortas revealed increased medial thickening (Figures 1C–1E) associated with disrupted elastic fibers (Figure 1D), an unusual finding often observed after vascular injury. The medial thickening was associated with VSMC hyperplasia (Figure 1F) but no significant changes in aortic lumen size (Figure 1G). *LRP6*^{R611C} VSMCs exhibited considerably lower expression of the contractile proteins—SM α-actin and SM-MHC—and increased expression of undifferentiated VSMC marker vimentin compared to WT, assayed by immunostaining (Figure 1H) and western blot analysis (Figure 1I). *LRP6*^{R611C} aortic VSMCs showed decreased expression of myocardin (Figure S1A) and increased phosphorylation/activation of ELK1 (Figure S1B), which act as transcriptional activator and suppressor of SMC genes, respectively. SM α-actin mRNA levels were lower in isolated *LRP6*^{R611C} VSMCs, which further reduced upon PDGF-BB stimulation, as compared to WT (Figure 1J). Furthermore, *LRP6*^{R611C} VSMCs showed increased proliferation upon PDGF-BB stimulation, as compared to WT (Figure 1K).

Given that PDGF signaling is a master regulator of VSMC differentiation, we next examined the activity of this pathway. *LRP6*^{R611C} mice exhibited increased expression of PDGF receptors β and α as well as their ligands PDGF-BB and -AA compared to WT mice both in aortic media (Figures 2A–2C) and isolated primary VSMC (Figure 2D). In addition, there was increased expression of IGF1 in the aortic media of *LRP6*^{R611C} mice compared to WT (Figure 2E). Study of the crystal structure of the LRP6 has shown that R611C substitution results in relaxation of the EGF2 domain (Cheng et al., 2011), determining which can explain its reduced affinity for ligands. We have previously shown that the *LRP6*^{R611C} mutation causes reduced, but not a complete ablation of, LRP6 signaling, and signaling can be rescued by high levels of ligand (Mani et al., 2007). To determine whether activation of LRP6 would reduce the growth factor levels in *LRP6*^{R611C} mice aorta, recombinant mouse (rm) Wnt3a was administrated to *LRP6*^{R611C} and WT mice on alternate days for 3 weeks. This resulted in dramatic reduction of PDGFRβ, PDGF-BB, -AA, and IGF-1 expression in the aortic media of *LRP6*^{R611C} mice (Figures 2A–2C and 2E). Most strikingly, this treatment caused significant reduction of the aortic medial thickening (Figure 2F). Taken together, these findings indicated that altered LRP6 function promotes VSMC phenotypic transformation by enhancing growth factor levels.

LRP6 Transcriptional Regulation of Sp1 and Its Effect on VSMC Differentiation

The upregulation of vimentin and growth factor ligands and receptors in *LRP6*^{R611C} VSMCs indicated a change in the function of a master regulator of VSMC differentiation. A common feature among these proteins is that they are all regulated by Sp1, a ubiquitously expressed transcription factor and an established regulator of VSMC plasticity (Lin et al., 1992; Park et al., 1998; Zhang et al., 2003). Strikingly, there was a dramatic increase in expression of Sp1 protein (Figures 3A and 3B) and mRNA (Figure 3C) in *LRP6*^{R611C} VSMCs compared to WT. These findings strongly suggested transcriptional suppression of *Sp1* by LRP6. To test this hypothesis, we stimulated primary VSMCs with rmWnt3a (50 ng/ml), which resulted in significant reduction of Sp1 (Figure 3C). These changes were associated with an increase in SM α-actin mRNA levels (Figure 3D) in WT and *LRP6*^{R611C} VSMCs. Most remarkably, administration of rmWnt3a in *LRP6*^{R611C} mice also resulted in decreased expression of Sp1 (Figure 3A) and Sp1 target genes such as PDGF ligands, PDGFRβ, and IGF-1 (Figures 2A–2C and 2E) and increased expression of the contractile proteins SM α-actin and SM-MHC (MYH11; Figure 3E) in the aorta.

LRP6 Regulation of Sp1 Is Mediated by TCF7L2

Polymorphisms in the Wnt effector *TCF7L2* gene have been associated with the prevalence and severity of CAD (Sousa et al., 2011). DNA array-based genome-wide analysis combined with reporter assays has identified multiple TCF7L2-binding sites in *Sp1* promoter (Hatzis et al., 2008). There was decreased expression of TCF7L2 (Figures 3F and 3G) and both total and nuclear and cytosolic β-catenin (Figures 3F, S2A, and S2B) in primary VSMCs and the aortic media of *LRP6*^{R611C} mice compared to WT. Whereas rmWnt3a treatment (2 hr) had only modest effects on β-catenin expression in *LRP6*^{R611C} mice (Figure 3F), it significantly increased TCF7L2 expression in *LRP6*^{R611C} VSMCs both in vitro and in vivo (Figures 3F and 3G). The treatment time course with Wnt3a showed that TCF7L2 expression steadily increases and peaks at 8 hr and Sp1 expression reduces and reaches its lowest level at 8 hr (Figure S2E). We then examined the potential role of TCF7L2 in inhibiting Sp1 expression in *LRP6*^{R611C} VSMCs. TCF7L2 was overexpressed in *LRP6*^{R611C} VSMCs, and its effect on Sp1 mRNA expression was examined. TCF7L2 overexpression resulted in downregulation of Sp1 transcription (Figure 3H); reduced expression of Sp1 downstream targets PDGF-AA, PDGFRβ, and vimentin (Figure 3I); and upregulation of SM α-actin (Figure 3H). Taken together, these findings indicate that TCF7L2 acts as a transcriptional suppressor of Sp1.

To explore whether TCF7L2 directly suppresses Sp1 through DNA binding, a ChIP assay was carried out. *Sp1* gene contains several conserved TCF-binding motifs T-C-A-A-A-G (Gustavson et al., 2004; Hatzis et al., 2008). The assay revealed that one motif

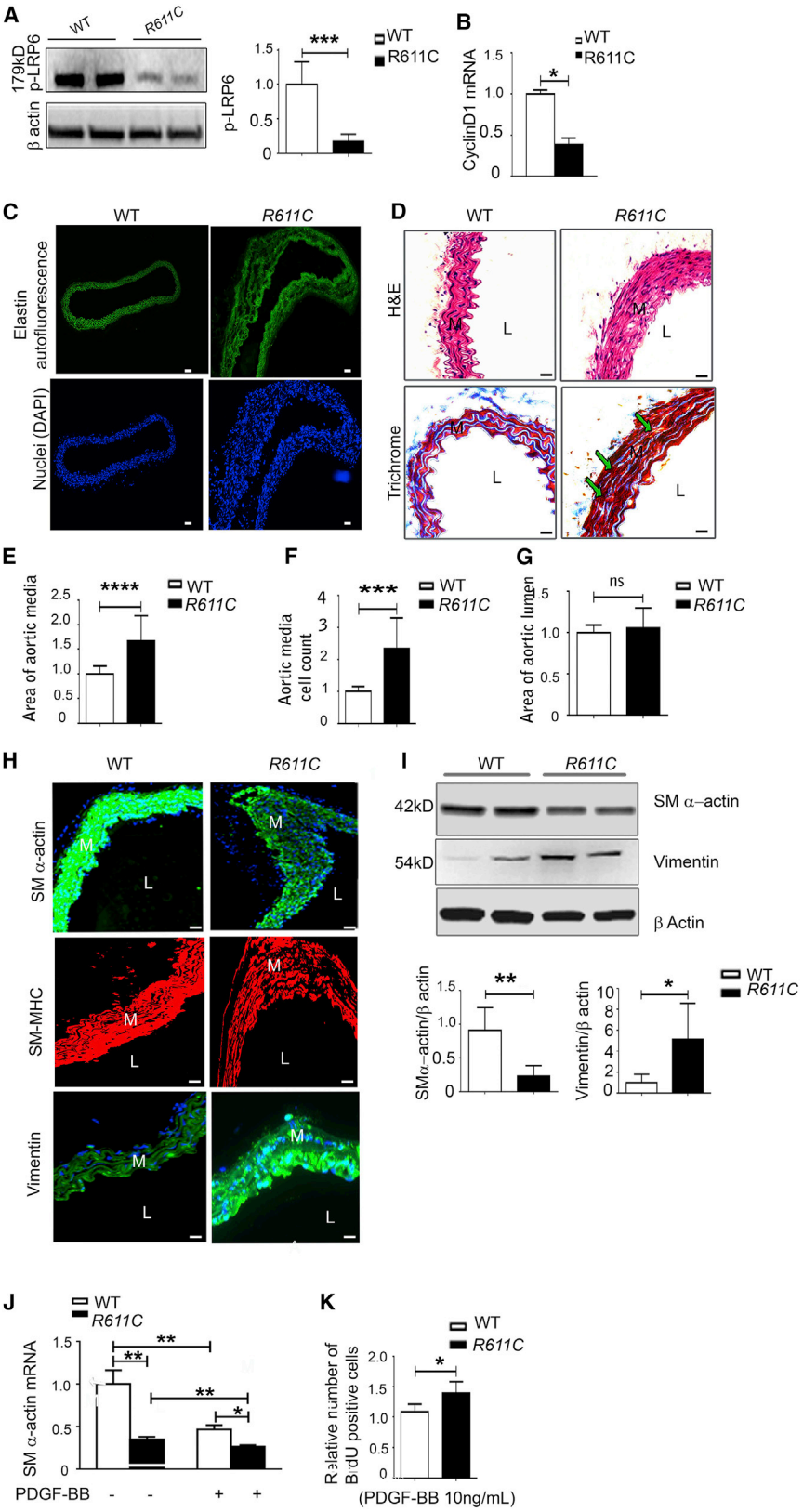

Figure 1. Impaired Wnt Signaling in *LRP6*^{R611C} Mice Causes Vascular Smooth Muscle Cell Proliferation

(A) Western blot of p-LRP6 levels in *R611C* and WT VSMC.

(B) Cyclin D1 mRNA in *R611C* and WT VSMCs.

(C) Elastin autofluorescence (green) and nuclei (blue) staining of aorta.

(D) H&E and trichrome staining showing medial thickening, increased cellularity, and disrupted elastic laminae (green arrows in *R611C* aorta versus WT, respectively; n = 10).

(E–G) Quantification of aortic media cross-sectional area, cell count, and lumen size (n = 10).

(H) Immunofluorescence staining of aorta for SM α-actin (green), SM-MHC (red), and vimentin (green; n = 5).

(I) Western blot of SM α-actin and vimentin in VSMC.

(J) SM α-actin mRNA expression of WT and *R611C* VSMCs, baseline and upon PDGF-BB stimulation.

(K) BrdU-positive cells WT and *R611C* VSMCs, baseline expression and upon PDGF-BB stimulation.

L, lumen; M, media; p- LRP6, phosphorylated LRP6; R611C, *LRP6*^{R611C}; WT, wild-type. Quantification of western blots and qPCR were performed on data from three independent experiments. Data represent means ± SD. The scale bar represents 25 μm. ****p < 0.0001; **p < 0.005; *p < 0.05. See also Figure S1.

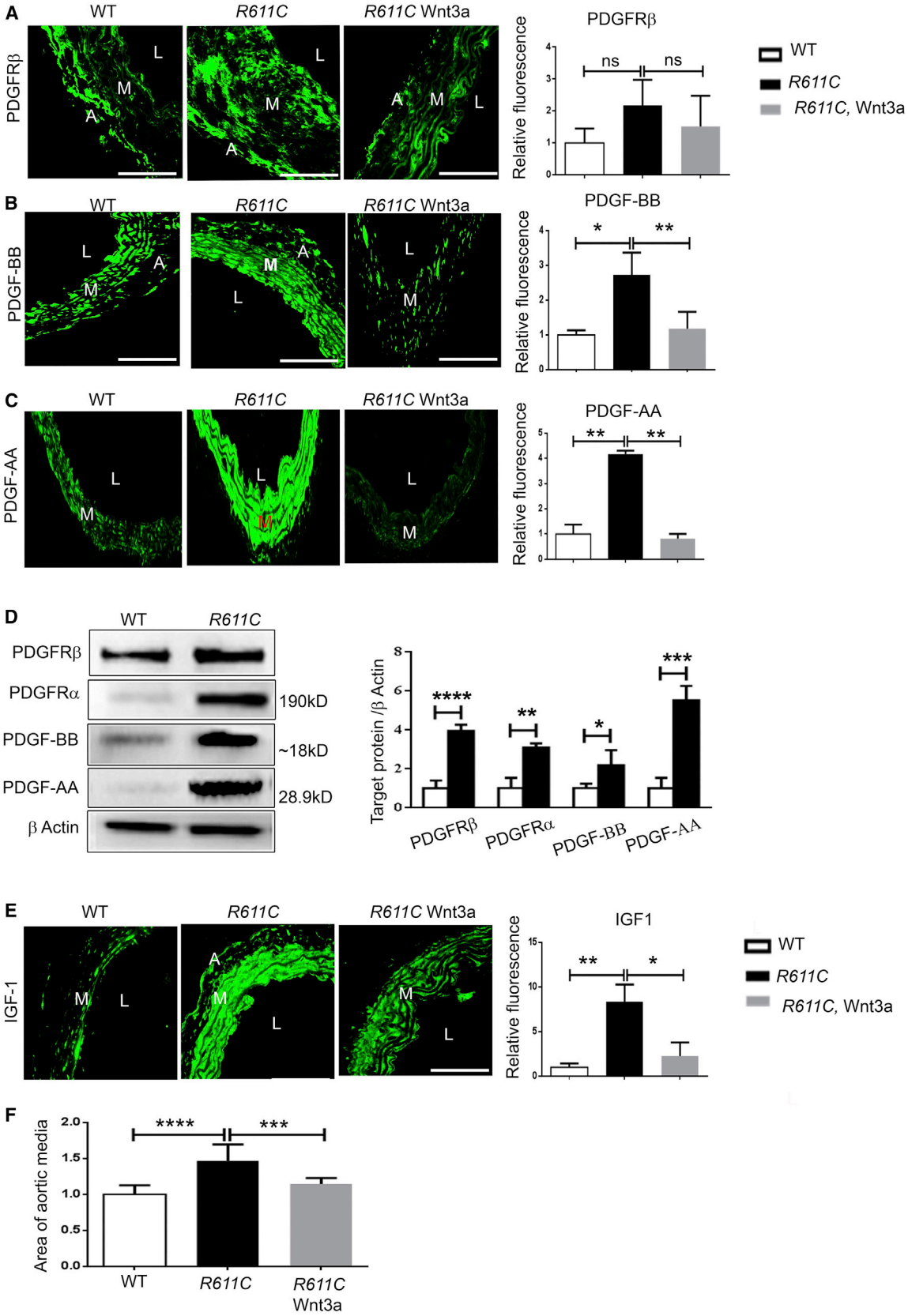

(legend on next page)

downstream from transcription initiation site exhibits enhanced binding to TCF7L2 upon Wnt3a activation (Figure 3J). An earlier study had shown that the position of T-cell-factors-binding motifs upstream or downstream of transcription start sites may determine whether T cell factors act as activator or suppressor (Gustavson et al., 2004). Taken together, our data suggest that TCF7L2 binding of T-C-A-A-A-G motif downstream from transcription initiation site in Sp1 gene is activated by Wnt3a and possibly plays a role in inhibition of its transcription.

Loss of TCF7L2 in *LRP6^{R611C}* Is Caused by Increased Non-canonical Wnt-Signaling Activity

LRP6^{R611C} aortic media exhibited reduced canonical Wnt signaling as shown by reduced total and phosphorylated LRP6 and cyclinD1 expression levels (Figures 4A–4C). Recent studies have shown that impaired activation of LRP6 can result in increased activation of non-canonical Wnt-signaling pathways. A major difference between canonical and non-canonical Wnt-signaling pathways is that the former increases β-catenin nuclear localization and promotes TCF7L2 activity and expression (Singh et al., 2013a; Wang et al., 2015), whereas the latter wields opposite effects by Nemo-like kinase (NLK)-mediated phosphorylation and ubiquitination of TCF7L2 (Ishitani et al., 1999). Reduced TCF7L2 expression in *LRP6^{R611C}* VSMCs suggested a shift toward increased activity of the non-canonical Wnt pathway at the expense of canonical Wnt. Extensive analysis of non-canonical Wnt-signaling pathway revealed increased activation of the non-canonical RhoA, JNK, and NLK in aortic media (Figures 4D–4F) and aorta lysates (Figure 4G) of *LRP6^{R611C}* versus WT mice. Administration of rmWnt3a to *LRP6^{R611C}* mice resulted in increased LRP6 phosphorylation (Figure 4B), enhanced TCF7L2 (Figure 3F), and cyclinD1 (Figure 4C) expression and reduced activities of non-canonical Wnt pathways RhoA, JNK, and NLK (Figures 4D–4F). NLK binds to and phosphorylates TCF7L2 at threonine residues T178 and T189 (Ishitani et al., 2003). In absence of a reliable antibody, we co-immunostained aortic cross-sections with phosphorylated threonine and TCF7L2-specific antibodies. The immunostaining images showed significant co-localization of TCF7L2 and phosphothreonines, suggestive of increased TCF7L2 threonine phosphorylation in *LRP6^{R611C}* as compared to wild-type mice (Figure S2C). This finding was also confirmed by TCF7L2 immunoprecipitation and western blot analysis using anti-phosphothreonine antibody (Figure S2D). In addition, there was an overall increase in phosphorylated threonine staining in *LRP6^{R611C}* aorta as compared to wild-type mice, which is consistent with increased growth-factor-signaling activity. These results establish a link between LRP6, non-canonical Wnt, and TCF7L2 in the vasculature and underlie their importance in vascular integrity.

Increased Neointima Formation Post-Carotid-Artery Injury in *LRP6^{R611C}* Mice Is Rescued by Wnt3a

VSMC proliferation is a typical response in following carotid artery injury and a major cause of neointima formation in diverse disease states. We next used guide wire carotid injury in *LRP6^{R611C}* mice to determine whether *LRP6^{R611C}* augments neointima formation and whether Wnt3a treatment would rescue it. Three weeks post-injury, *LRP6^{R611C}* carotid arteries showed significant neointima formation compared to WT mice, which had minimal neointima (Figures 5A and 5B). Although LRP6 plays a critical role in regulation of endochondral metaplasia, staining of the injured carotid artery with Alizarin Red did not reveal any evidence for the same (data not shown). The hyperplastic response of the injured *LRP6^{R611C}* carotid was accompanied by reduced TCF7L2 (Figure 5C) and increased Sp1 expression (Figure 5D) and consequently low expression levels of SM α-actin (Figure 5E) in *LRP6^{R611C}* mice carotid arteries. Consistent with our earlier results, administration of i.p. rmWnt3a resulted in significant protection against neointima formation in injured *LRP6^{R611C}* mice as compared to untreated mice (Figures 5A–5D). This finding correlated with the rise in TCF7L2 (Figure 5C) and fall of Sp1 expression levels (Figure 5D) compared to untreated *LRP6^{R611C}* mice.

LRP6^{R611C} Mice on High-Cholesterol Diet Exhibit Arterial Neointima Formation and Coronary Artery Disease

The most striking finding of our study was the development of a dramatic form of CAD in *LRP6^{R611C}* mice fed with high-cholesterol/high-fat diet for 10 months, despite only modest elevation of VLDL/LDL in these mice (Go et al., 2014). The aortic root and coronary arteries of *LRP6^{R611C}* mice showed extensive neointima formation (Figures 6A and 6B), which stained intensely positive for SM α-actin (Figure 6C). This observation was in contrast to our earlier findings in *LRP6^{R611C}* mice on chow diet and suggested maturation of VSMCs in later stages of the disease. Surprisingly, the neointima exhibited paucity of F4/80-positive cells (Figure 6D) and no significant changes in plasma cytokine levels between *LRP6^{R611C}* versus WT mice (Figure S3C). Furthermore, there were increased vimentin-positive cells in all aortic layers (Figure S3A).

The lamina media in *LRP6^{R611C}* mice was remarkably small, which could be in part explained by migration of VSMCs into intima. We speculate that the undifferentiated VSMCs proliferate and migrate to intima and ultimately undergo differentiation, a hypothesis that can only be verified by fate-mapping studies. In addition, there was increased apoptosis by TUNEL staining in the tunica media (and adventitia) of the coronary artery and aortic root of *LRP6^{R611C}* versus WT mice, which could be also accountable for the thinning of the tunica media (Figure S3B,

Figure 2. Impaired Wnt Regulation of Growth Factor Expression in *LRP6^{R611C}* Mice

(A–C) Immunostaining for (A) PDGFRβ, (B) PDGF-BB, and (C) PDGF-AA in aortic cross-sections of *R611C* and WT mice (n = 7 each).

(D) Western blot analysis of PDGFRβ, PDGFRα, PDGF-BB, and PDGF-AA in *R611C* and WT primary VSMC and its quantification from three independent experiments.

(E) IGF-1 expression in *R611C* and WT mice aorta (n = 7 each).

(F) Aortic media area quantification in WT and *R611C* mice (n = 7 each).

A, adventitia; *RC* and *R611C*, *LRP6^{R611C}*. Data represent mean ± SD. The scale bar represents 25 μm. **p < 0.02; ****p < 0.0001.

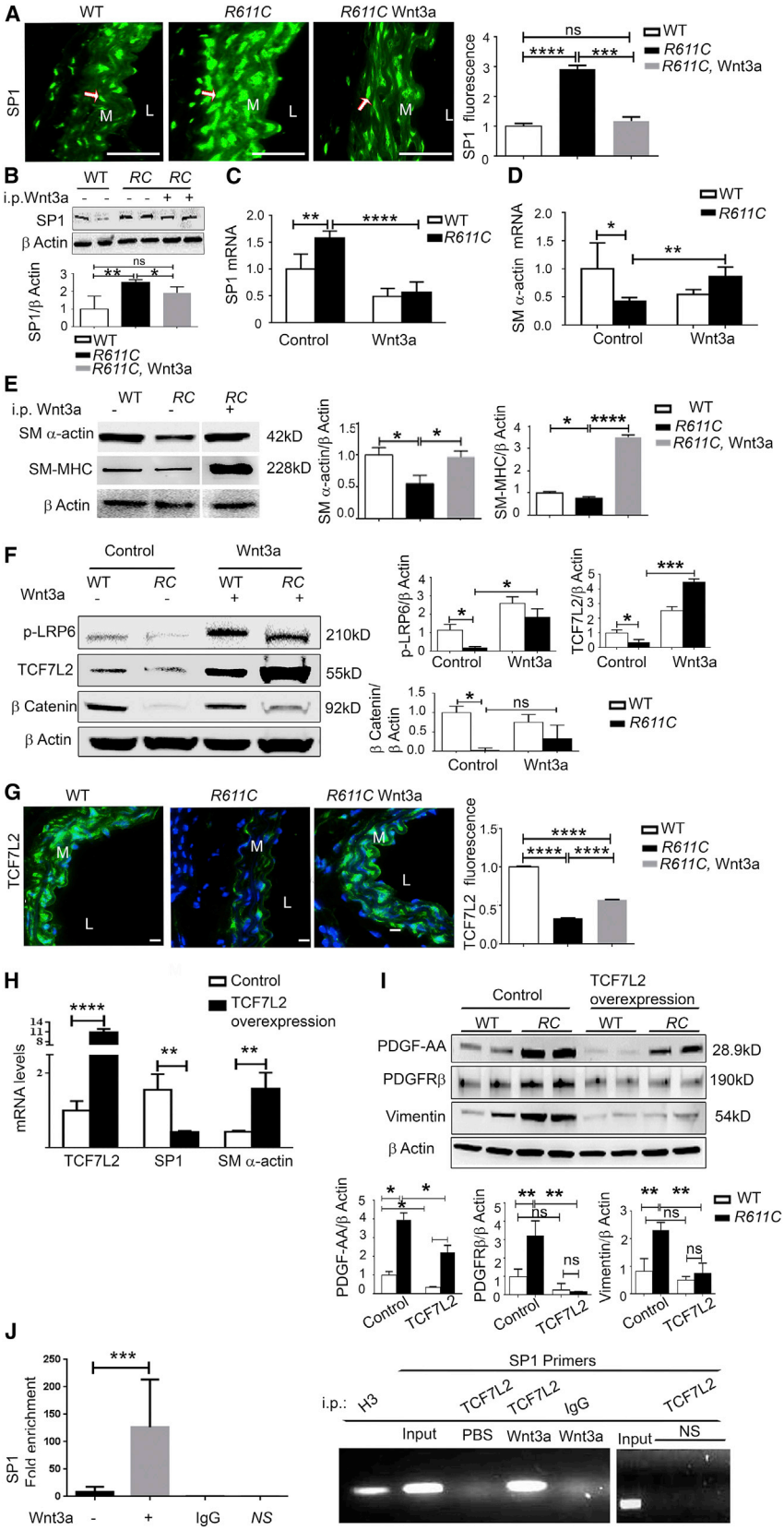

Figure 3. Impaired TCF7L2-Dependent Transcriptional Regulation of Sp1 in *LRP6*^{R611C} Mice Underlies Loss of VSMC Differentiation

(A) Sp1 expression (arrows) by immunostaining in aorta of *R611C* and WT mice (n = 7 each).

(B) Sp1 protein levels in aorta lysates from *R611C* and WT mice by western blot.

(C) SP1 mRNA levels (**p = 0.001; ****p < 0.0001) in primary VSMC of *R611C* and WT.

(D) SM α-actin mRNA levels in primary VSMC of *R611C* and WT (*p = 0.02; **p = 0.003).

(E) SM α-actin and SM-MHC protein levels in aortic lysates from *R611C* and WT mice.

(F) Western blot showing changes in LRP6 phosphorylation, TCF7L2, and β-catenin levels in Wnt3a-stimulated VSMC.

(G) TCF7L2 expression (arrows) in *R611C* and WT mice aorta by immunostaining.

(H) mRNA expression of Sp1 and SM α-actin in *R611C* primary VSMCs, with or without TCF7L2 overexpression (****p < 0.0001; **p = 0.005).

(I) Western blot of Sp1 target genes PDGF-AA, PDGFRα, and vimentin in control and TCF7L2-overexpressing *R611C* and WT VSMCs.

(J) ChIP assay demonstrating TCF7L2 binding of T-C-A-A-A-G motif in Sp1 gene upon Wnt3a stimulation (***p < 0.001). IF data are representative of n = 7 mice per group; quantification of western blot and qPCR data are from three independent experiments.

Error bars show mean ± SD. The scale bar represents 25 μm. NS, non-specific target. See also Figure S2.

top row). The increase in apoptosis perfectly correlated with the overexpression of Sp1, which is a strong driver of apoptosis (Deniaud et al., 2009).

To further examine the role of VSMC phenotype switching on atherosclerotic lesion development, *LRP6*^{R611C} mice were crossbred onto low-density lipoprotein receptor knockout (LDLR−/−) background and were fed HCD for 4 months. En face aorta preparations of *LRP6*^{R611C}; LDLR−/− mice showed greater than 2-fold increase in atherosclerosis burden compared to LDLR−/− mice (48% versus 20%; Figure 7A). *LRP6*^{R611C} mice en face aorta preparations did not show any positive staining with Sudan IV (data not shown). Accordingly, there was a significant increase in atherosclerotic lesion size in the aortic roots of *LRP6*^{R611C}; LDLR−/− versus LDLR−/− mice (Figure 7B). Examination of atherosclerotic lesions in the aortic root cross-sections of *LRP6*^{R611C}; LDLR−/− mice, however, showed once again increased presence of SM α-actin and vimentin-positive cells (Figure 7C) and increased apoptosis (Figure S3B, bottom row) compared to LDLR−/− mice. In addition, the coronary arteries of the *LRP6*^{R611C}; LDLR−/− mice were significantly enlarged and showed either luminal narrowing or occlusion, primarily accounted for by SM α-actin-positive cells (Figure 7D). There was enhanced elastin staining in the atherosclerotic lesions of *LRP6*^{R611C}; LDLR−/− versus LDLR−/− mice, providing further evidence for the presence of VSMCs in the lesion (Figure 7G). Remarkably, the atherosclerotic lesions in *LRP6*^{R611C}; LDLR−/− mice exhibited significantly fewer F4/80- or CD36-positive cells compared to LDLR−/− mice (Figures 7H and 7I). Accordingly, plasma cytokine profiling of *LRP6*^{R611C}; LDLR−/− mice showed no significant difference in the plasma levels of inflammatory cytokines IL1α/β, IL6, IL10, IL17, IFNγ, and TNFα but significantly lower plasma levels of MCP-1, a critical chemokine for monocyte recruitment and activation as compared to LDLR−/− mice (Figure 7K). In comparison, there was an increase in the number of CD3+ T cells (Figure 7J) and IL6 levels (Figure S3D) in the atherosclerotic lesions of *LRP6*^{R611C};LDLR−/− versus LDLR−/− mice. No significant changes in MMP9, another inflammatory marker, were observed (Figure S3C). We further examined the causes of increased atherosclerotic burden of LDLR−/− mouse by the mutant allele in absence of increased inflammation. Earlier studies by our group had shown increased cholesterol synthesis in diverse human and mice cell types expressing *LRP6*^{R611C}. Thus, we compared the free cholesterol content of the aortic wall between *LRP6*^{R611C} and WT mice as well as *LRP6*^{R611C}; LDLR−/− versus LDLR−/− mice. The result was striking, as the entire aortic wall in *LRP6*^{R611C} and *LRP6*^{R611C}; LDLR−/− mice was positive for filipin as compared to modest staining in WT and LDLR−/− mice (Figures S4A and S4B). Strikingly, *LRP6*^{R611C} VSMC expressed significantly higher HMGCR protein, despite greater cholesterol content compared to WT mice. Altogether, these findings suggested that VSMCs synthesize and accumulate free cholesterol and increase the atherosclerotic burden. Although it is widely accepted that VSMCs form protective fibrous caps and stabilize atherosclerotic lesions, we demonstrate here that they can also augment atherosclerotic burden by proliferation and expansion of neointima and generation of occlusive disease.

DISCUSSION

Despite intensive investigations over the past decades, progress in identification of novel CAD risk factors has been incremental. Aberrant Wnt signaling has recently emerged as a risk factor for CAD and diabetes (Go et al., 2014; Mani et al., 2007; Singh et al., 2013b; Wang et al., 2012; Xu et al., 2014). In this study, we report that the CAD-associated *LRP6*^{R611C} mutation causes increased non-canonical Wnt activation, alters VSMC phenotype, and leads to development of obstructive CAD in mice. This finding establishes the association between loss-of-function *LRP6* mutations and CAD in humans and implies a critical role of non-canonical Wnt in development of arterial disease.

There have been several lines of evidence in support of VSMCs lack of terminal differentiation (Gomez and Owens, 2012). Most recent studies have provided strong evidence for VSMC transdifferentiation into macrophages in atherosclerotic mouse models (Allahverdian et al., 2014; Feil et al., 2014). Lineage tracing of SMC in Apoe−/− mice has shown that large number of macrophages and MSCs in advanced atherosclerotic lesions are SMC derived (Shankman et al., 2015). The contribution of VSMCs to neointima formation in humans has been depicted by microscopic evidence of their migration through disrupted internal elastic lamina into the neointima (Schwartz et al., 1995). Most strikingly, the autopsy examination of coronary artery plaques in young men and women who had died from myocardial infarction have revealed massive proliferation of VSMCs in absence of inflammatory cells in nearly half of all cases (Farb et al., 1996; Virmani et al., 2000). This important clinical feature is rarely seen in mouse models of atherosclerosis. Our study in this novel mouse model of human mutation reveals medial and neointimal thickening, including occlusive lesions in the absence of excessive lipids or inflammation. This establishes the key role of VSMCs in CAD development and identifies LRP6 as critical regulator of their plasticity. These findings suggest cell-autonomous effect of LRP6. Nonetheless, LRP6 is ubiquitously expressed, and the effect of the mutant allele on the function of other cell types such as vascular endothelial cells and cells of myeloid lineage may have contributed to the disease. Several lines of evidence, however, support the important role of LRP6 in VSMCs. Of note, mice with VSMC-specific LRP6 knockout recently were shown to develop arterial calcification (Cheng et al., 2015). Interestingly, human mutation carriers have coronary artery calcification, but this trait was not observed in our mouse model.

Earlier in vitro studies had implicated both canonical and non-canonical Wnt in VSMC proliferation, but the underlying mechanisms were unclear. In the current study, we show that non-canonical Wnt regulation of VSMC plasticity is TCF7L2 dependent and is exercised through modification of Sp1 expression levels. A ChIP assay demonstrated TCF7L2 binding to Sp1 gene downstream from transcription initiation site upon Wnt3a stimulation differentiation. Sp1 is a ubiquitously expressed transcription factor that regulates a diverse array of cellular processes, including VSMC differentiation. JNK has been also shown to increase Sp1 transcriptional activity by promoting its phosphorylation (Tan and Khachigian, 2009). Thus, enhanced non-canonical Wnt activity in *LRP6*^{R611C} VSMCs may contribute to excess activity and availability of Sp1.

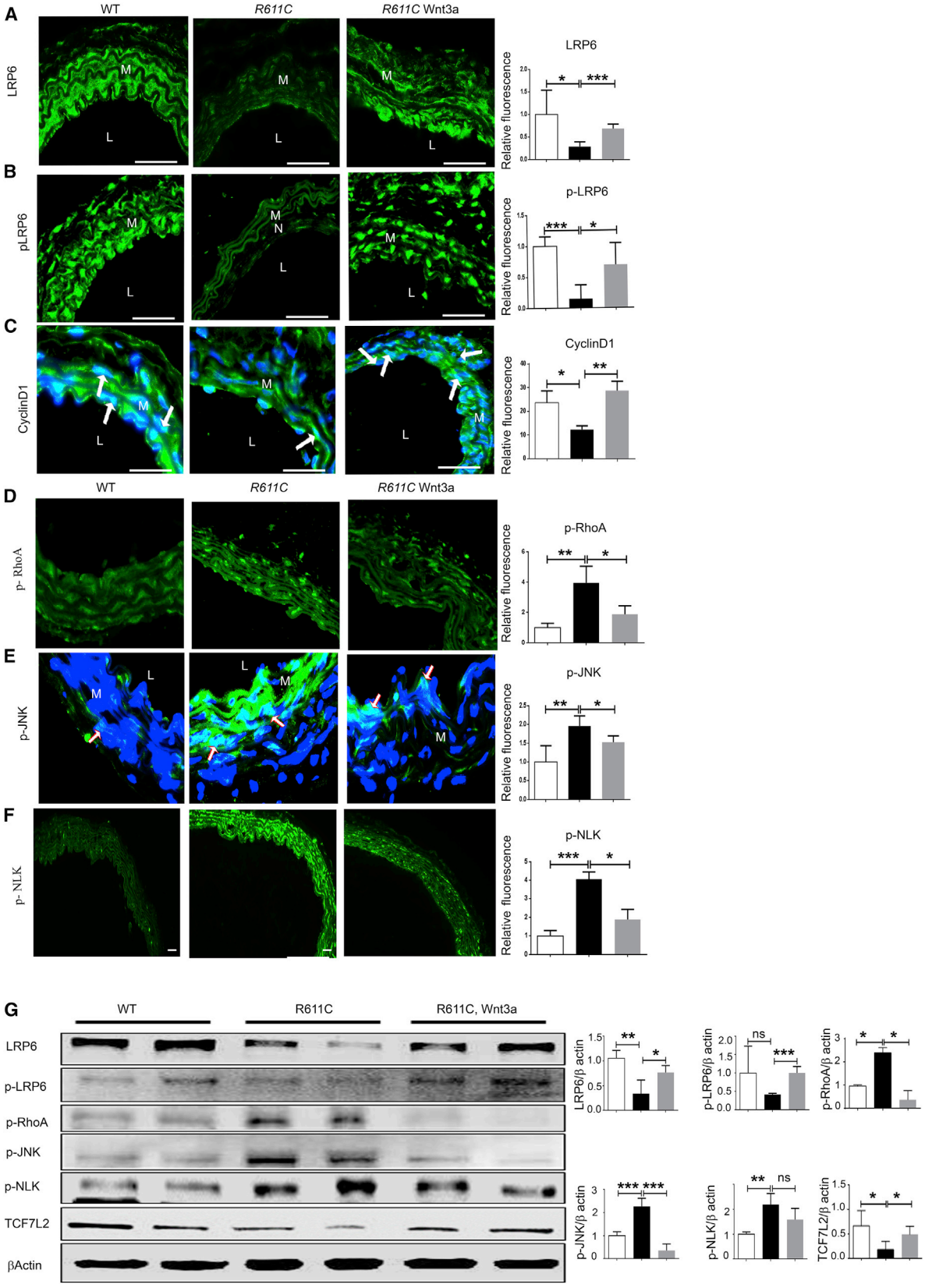

(legend on next page)

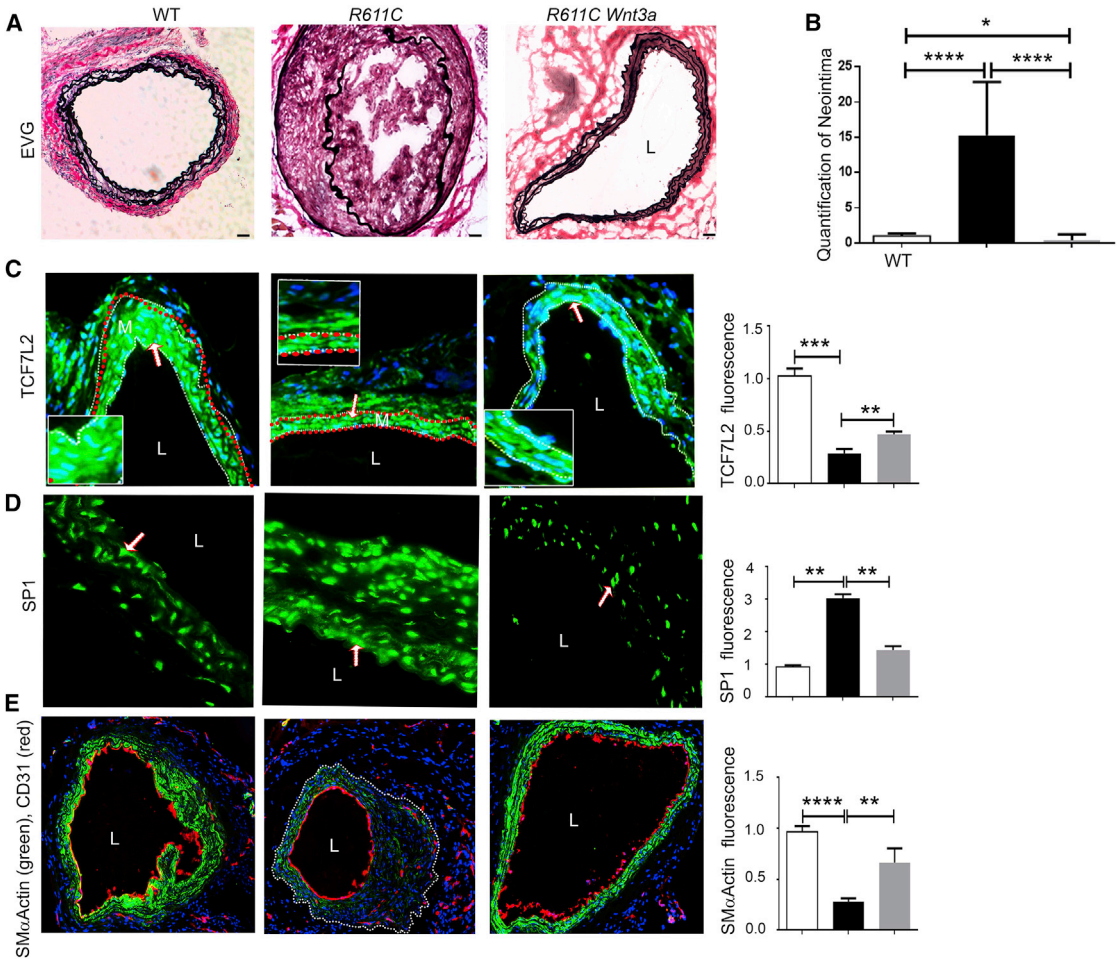

Figure 5. Wnt3a Rescues Post-Carotid-Injury Neointima Formation in *LRP6*^{R611C} Mice

(A) Elastin staining.

(B) Quantification of neointima formation (n = 7 each).

(C–E) IF staining of carotid for (C) TCF7L2 (arrows), (D) Sp1 (arrows), and (E) SM α-actin and CD31 (endothelium); dotted lines mark the area of carotid artery; in *R611C* and WT mice post guide wire injury with or without i.p. Wnt3a and its quantification (n = 7).

Dotted lines separate neointima from media. Error bars show mean ± SD. ****p < 0.0001; **p < 0.005; *p < 0.05. The scale bar represents 25 μm.

Common genetic variants in *TCF7L2* have been associated with the risk for diabetes and hyperlipidemia and coronary artery disease (Muendlein et al., 2011), indicating the broader role of this transcription factor in diverse cardiovascular disorders of the general population. TCF7L2 activation and expression is triggered by the canonical Wnt (Singh et al., 2013a) and is inhibited by non-canonical Wnt activation of NLK (Ishitani et al., 1999). NLK phosphorylates TCF7L2, which results in inhibition of its DNA binding and its subsequent targeting to ubiquitination and degradation. The rescue of the vascular phenotype by Wnt3a was associated with reduced phosphorylation and increased expression of TCF7L2, further highlighting the critical role of non-canonical Wnt in this process. Interestingly, VSMC calcification has been recently shown to be triggered by loss of LRP6 and increased activation of non-canonical Wnt (Cheng et al., 2015).

Certain Wnt ligands are specific for canonical versus non-canonical Wnt pathway, which are known to reciprocally inhibit each other (Nusse, 2012). Wnt3a has been surprisingly shown to activate both pathways, although the specific circumstances and the mechanisms had not been explored (Nalesso et al.,

Figure 4. Increased Activation of Non-canonical Wnt in *R611C* Mice and Its Rescue by Wnt3a

(A–F) Immunofluorescence of aortic sections demonstrating LRP6 (A); phosphorylated LRP6 (B); and cyclinD1 in aorta (arrows; C), p-RhoA (D), p-JNK (E; arrows), p-NLK (F), and its quantification in *R611C* and WT mice (n = 7 each).

(G) Western blot analysis of aorta lysate from mice treated with or without i.p. Wnt3a analyzed for LRP6 mediated non-canonical Wnt regulation, its effect on TCF7L2, and its quantification (n = 6).

The scale bar represents 25 μm. N, neointima; p, phosphorylated.

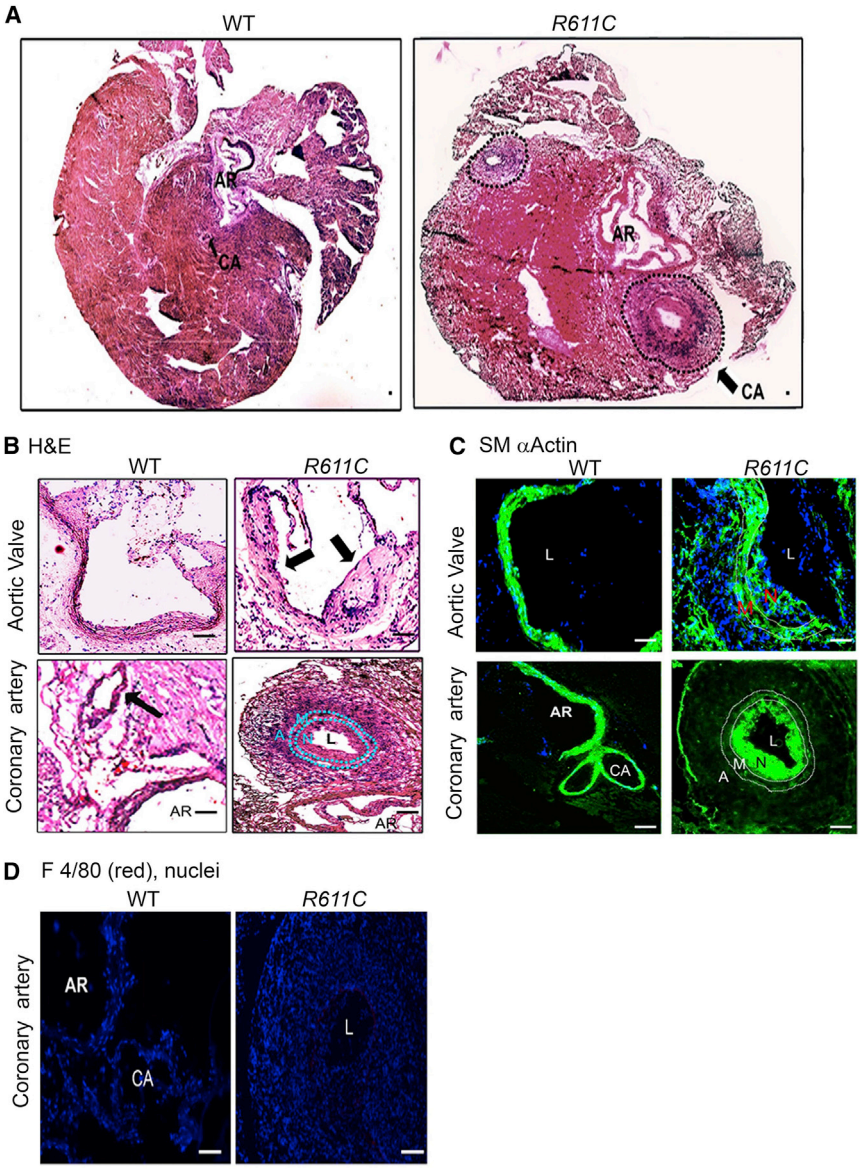

Figure 6. *LRP6*^{R611C} Mutation Induces Formation of Arterial Neointima on High-Cholesterol Diet

(A) Cross-sections of WT and *R611C* mice hearts on HCD showing hyperplasia of CA (delineated by dotted lines) and AR in *R611C* versus WT mice (arrows).

(B) H&E staining of AR and CA showing neointima formation (arrows).

(C and D) Immunofluorescence staining of the neointima of AR and CA for (C) SM α-actin (green; AR and CA) and (D) F4/80 (CA). Data are representative of n = 9 mice per group.

The scale bar represents 25 μm. AR, aortic root; CA, coronary artery. See also Figures S3 and S4.

2011). Our rescue studies in *LRP6*^{R611C} mice show the critical role of Wnt3a in regulation of non-canonical Wnt in the vessel wall. This rescue, as we have previously shown, is possible by larger Wnt3a dose to overcome reduced affinity of the mutant receptor for ligands. Our investigation of CAD development in humans and mice with *LRP6*^{R611C} mutation indicates the pathological role of excess non-canonical Wnt activity in the VMSC.

One unexpected finding of our study was reduced expression of macrophage markers F4/80, CD68, and MCP-1 in *LRP6*^{R611C}; LDLR−/− despite increased atherosclerotic burden compared to LDLR−/− mice. However, these findings are logical and consistent with the established role of Wnt signaling in monocyte/macrophage maturation and promotion of inflammatory response (Pereira et al., 2009). In comparison, there were increased CD3+ T cells in atherosclerotic lesion of *LRP6*^{R611C} LDLR−/− versus LDLR−/− mice. Earlier studies have shown that Wnt signaling is required for T cell proliferation arrest and negative regulation of regulatory T cells (Shen et al., 2013; van Loosdregt et al., 2013), and hence, loss of Wnt signaling in *LRP6*^{R611C} mice could explain increased T cell proliferation. There were also increased eotaxin levels in *LRP6*^{R611C}; LDLR−/− versus LDLR−/− mice, suggesting increased eosinophil activation. Increased eosinophil activation in patients with hypereosinophilia has been attributed to impaired Wnt signaling, measured by lower cyclin D1 and β-catenin levels. Interestingly, eotaxin has been shown to activate T cell infiltration, which may be another explanation for increased T cells in *LRP6*^{R611C}; LDLR−/− versus LDLR−/− lesions (Giannetti et al., 2014). Finally, increased T cell in *LRP6*^{R611C}; LDLR−/− versus LDLR−/− may have been contributed by increased IL-6, as IL-6 is known to promote T cell proliferation (Dienz and Rincon, 2009). The role of IL-6 in atherosclerosis, however, has been controversial and may be context dependent (Ait-Oufella et al., 2011). Nevertheless, contribution of CD3 and IL6 in *LRP6*^{R611C}; LDLR−/− needs further investigations. Another limitation of our study is that it does not answer the disparities in VSMC phenotype, i.e., undifferentiated VSMCs in the aortic wall and highly differentiated VSMCs in the coronary artery neointima and in atherosclerotic lesions. Based on recent studies, we believe these are VSMCs that show significant plasticity at different stages of the development. A definitive answer, however, can be provided by fate mapping in these mice.

In summary, the *LRP6*^{R611C} knockin mouse constitutes one of the very few known rodent models of CAD. This model animal recapitulates features of human lesions and demonstrates the critical role of VSMCs in pathogenesis of CAD. In this model, we were able to show that altered function of Wnt/LRP6/TCF7L2 axis can induce VSMCs plasticity and initiate vascular wall remodeling. These findings identify LRP6 and TCF7L2 as

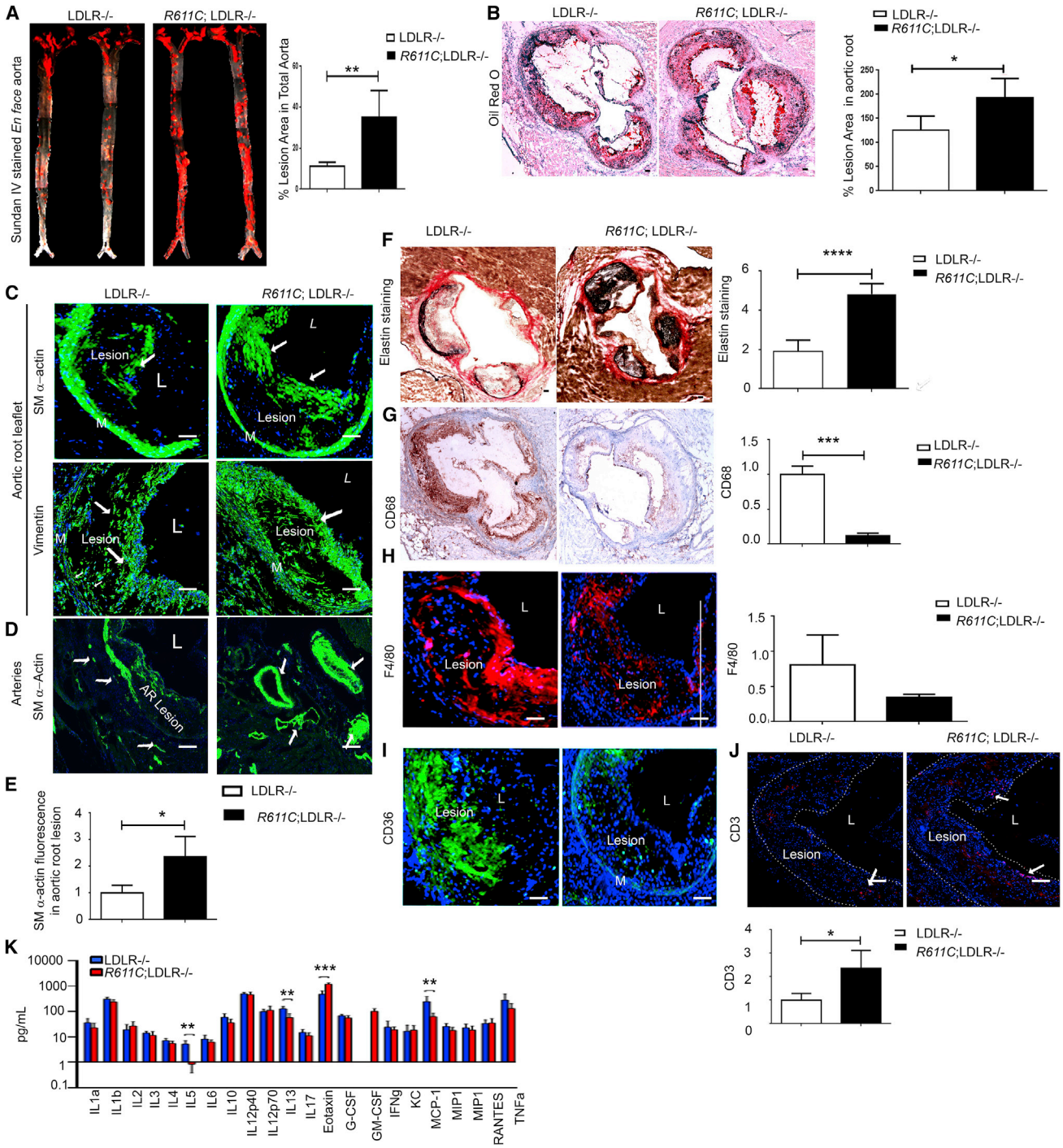

Figure 7. *LRP6*^{R611C} Mutation Increases the Atherosclerosis Burden in LDLR−/− Mice

(A) Atherosclerotic lesions (red) in en face aorta preparation of *LRP6*^{R611C}; LDLR−/− and LDLR−/− mice (n = 7 and 8).

(B) Atherosclerotic burden in AR.

(C) SM α-actin (top row, arrows) and vimentin (bottom row, arrows) staining of atherosclerotic lesions.

(D) SM α-actin staining showing enlarged and occluded arteries in *LRP6*^{R611C}; LDLR−/− versus LDLR−/− mice.

(E) Quantification of SM α-actin.

(F–J) Staining of atherosclerotic lesions in AR for (F) elastin (black), (G) CD68 (brown), (H) F4/80 (red), (I) CD36 (green), and (J) CD3 (red, arrows).

(K) Plasma cytokine profiling of *LRP6*^{R611C}; LDLR−/− versus LDLR−/− mice. Data represent mean ± SD.

The scale bar represents 25 μm. *p = 0.02; **p < 0.01; ***p < 0.001. See also Figure S4.

regulators of vascular wall integrity and as potential targets for the pharmacotherapy of coronary artery disease.

EXPERIMENTAL PROCEDURES

Animals

Animal procedures were as per approved protocol of Yale University Institutional Animal Care and Use Committee. Generation of homozygous *LRP6*^{R611C} and *LRP6*^{R611C}; LDLR−/− mice were previously described (Go et al., 2014). All mice used for the studies are homozygous and are referred to as either as *LRP6*^{R611C} in the text or *R611C* or *RC* mice in the figures. All mice were fed ad libitum and housed at constant ambient temperature in 12 hr light, 12 hr dark cycle. For high-cholesterol diet studies, at 6–8 weeks of age, the mice were fed high-cholesterol diet (40% fat, 1.25% cholesterol, and 0.5% cholic acid) ad libitum (Research Diets) for 4 or 10 months.

Chemicals and Antibodies

Protease inhibitor cocktail (P8340), phosphatase inhibitor cocktail (P2850), Sudan IV, and Oil red O were purchased from Sigma-Aldrich. Cell lysis buffer (9803) and antibodies for LRP6, p-LRP6(S1490), β-actin, PDGFRβ, p- PDGFRβ (y751/y771), and cKit were all purchased from Cell Signaling Technology. PromoFectin (PK-CT-2000-100) was purchased from Promokine. Wnt3a was from R&D Systems; DMEM, fetal bovine serum (FBS), penicillin streptomycin cocktail, Trypsin-EDTA solution, and TRIzol were purchased from GIBCO/Invitrogen; polyvinylidene fluoride membranes from Bio-Rad Laboratories; and Filipin stain from Cayman Chemical. Antibodies for PDGFRα, β-catenin, TCF7L2, SP1, CD3, and protein A/G agarose gel were purchased from Santa Cruz Biotechnology. Antibodies for PDGF-AA/-BB, F4/80, αSMA, and SM-MHC were purchased from Abcam, CD31 antibody from BD PharMingen, and secondary fluorescence tagged antibodies from Invitrogen.

Immunohistochemistry and Immunofluorescence

Immunofluorescence staining was performed on 5-μm frozen sections, and fluorescence was measured using Nikon Eclipse80i using same laser output, gain, and offset for each set of antibody tested. For atherosclerosis studies, whole aorta was trimmed off extraneous tissues and placed in formaldehyde sucrose solution and then pinned on wax pan and stained with Sudan IV and imaged. Aortic root sections were stained with Oil red O and. Images were quantified with Image J.

VSMC Isolation and Culture

Isolation of aortic VSMCs was carried out as previously described (Ray et al., 2001). VSMCs were maintained in DMEM (4.5g/l glucose, glutamine, and 100 mg/l sodium pyruvate) supplemented with 20% FCS, 100 U ml^{-1} penicillin, and 100 μg ml^{-1} streptomycin. For phosphorylation studies, cells were starved for 3 hr in 0.2% FBS containing DMEM and were treated as follows: PDGF-BB at 10 ng/ml for 15 min and Wnt3a (50 ng/ml) for 1 hr prior to PDGF-BB stimulation. For Wnt3a-dependent LRP6 phosphorylation and downstream targets, cells were starved for 3 hr in 0.2% FBS containing DMEM and were treated with Wnt3a for 2 hr. For mRNA studies, the cells were starved overnight in 0.2% FBS containing DMEM and treated with PDGF-BB (10 ng/ml) or Wnt3a (50 ng/ml) for 8 hr. For time course Wnt3a studies, cells were starved overnight in 0.2% FBS containing DMEM and treated with Wnt3a up to 8 hr.

In Vitro TCF7L2 Overexpression

Primary VSMCs were transfected with TCF7L2 plasmid (11031; Addgene) using PromoFectin transfection reagent according to the manufacturer's instructions. Briefly, 1 μg of TCF7L2 plasmid DNA or empty vector control plasmid DNA were diluted in 50 μl of Opti-MEM, were mixed with 2 μl of PromoFectin solution diluted in 50 μl of Opti-MEM, and incubated for 30 min at room temperature. The plasmid DNA solution was then added dropwise into VSMC culture in antibiotic free medium. After 5 hr, the medium was replaced with fresh antibiotic free medium. After 48 hr of transfection, cells were starved overnight and harvested for analysis.

ChIP Assay

Chromatin immunoprecipitation (ChIP) assay was performed according to the manufacturer's instructions (Pierce Agarose ChIP kit; 26156). Briefly, the chromatin/DNA protein complexes were prepared from mouse aortic smooth muscle cells treated with vehicle (PBS with 0.1% BSA) or Wnt3a (50 ng/ml) for 8 hr. Chemical crosslinking of DNA proteins was carried out using 1% formaldehyde for 10 min at room temperature and followed by addition of glycine solution. Cells were scraped into cold PBS containing Halt cocktail proteinase inhibitor. The cell suspension was centrifuged and the pellet was lysed and nuclei was digested using micrococcal nuclease to digest DNA to a length of approximately 200–1,000 bp. Supernatant containing the digested chromatin was incubated with appropriate ChIP-grade TCF-4 (TCF7L2) antibody (sc-8631; Santa Cruz Biotechnology) for immunoprecipitation overnight at 4°C with rotation, followed by ChIP-grade protein A/G agarose beads and incubation for 1 hr at 4°C with rotation. Anti-H3 antibody and β-actin primers were used as a positive control for assay technique and reagent integrity. The agarose resin was washed using buffers supplied with the kit. The eluted DNA was purified and analyzed by PCR to determine the binding of TCF7L2 to Sp1. The positions of TCF7L2-binding site in mouse Sp1 gene were determined (consensus sequence: TCAAAG; Hatzis et al., 2008). The following primers were used to amplify the binding region: forward 5′- TGCAGCAG AATTGAGTCACC-3′ and reverse 5′- CAGCCACAACATACTGCCCAC-3′. The primer sequences for β-actin promoter were forward 5′-GAGGGGAG AGGGGGTAAA-3′ and reverse 5′-GAAGCTGTGCTCGCGG-3′. Real-time PCR amplification was performed using iQ SYBR Green Supermix (Bio-Rad) and Eppendorf Mastercycler RealPlex2.

Carotid Artery Guide Wire Injury and Intraperitoneal rmWnt3a Administration

Mice were injected with 25 mg/kg i.p. rmWnt3a every other day for 3 weeks beginning 1 day prior to carotid wire injury. Similarly, control mice group received equal volumes of carrier buffer, in which rmWnt3a was dissolved. The carotid artery guide wire injury was performed as previously described (Wang et al., 2009). Three weeks post-injury, mice were euthanized and injured carotid arteries were excised from the arteriotomy site of external left carotid artery, including the internal left carotid artery and approximately 1 cm of left common carotid artery. Similarly, right common carotids were harvested and used as uninjured controls. The arteries were embedded in OCT; serial tissue sections (5 μm) were obtained from left and right common carotid arteries, starting at the bifurcation (to external and internal carotids); and immunofluorescence, IHC, and morphometric analyses were performed. Neointima formation was measured in ten sections (50 μm apart) using images obtained by a bright-field microscope and quantified using ImageJ software (NIH). Aorta and aortic roots were also harvested for studying Wnt3a effects on *LRP6*^{R611C} as compared to the controls by immunoblotting and immunofluorescence studies.

Immunoblotting

Whole-cell lysates of primary VSMCs were separated by electrophoresis, transferred to PVDF membrane, and probed using target primary antibodies followed by appropriate HRP-conjugated secondary antibodies. Blots were visualized using chemiluminescence reagents, imaged with Bio-Rad gel doc system, and quantified with Image J software.

Real-Time PCR

Total RNA was isolated from primary VSMC culture using TRIzol, and cDNA was generated using the High Capacity cDNA Reverse Transcription Kit (Applied Biosystems) according to the manufacturer's instructions. Real-time PCR amplification was performed using specific primers and iQ SYBR Green Supermix in Eppendorf Mastercycler RealPlex2. Reactions were performed in quadruple with a β-actin internal control. Relative quantification of mRNA levels was expressed as fold increase relative to the control. The following mouse primer sequences were used for qRT-PCR:

SM α-actin forward: 5′- CAGCTATGTGTGAAGAGGAAGACA-3′
SM α-actin reverse: 5′-CCGTGTTCTATCGGATACTTCAG-3′
Sp1 forward: 5′- CTGGTGGGCAGTATGTTGTG-3′

Sp1 reverse: 5′-TTGGTTTGCACCTGGTATGA-3′
CyclinD1 forward: 5′-GCCTCTAAGATGAAGGAGACCA-3′
CyclinD1 reverse: 5′-AGGAAGTGTTCGATGAAATCGT-3′

Apoptosis Detection

To detect apoptosis, aortic root cross-sections were fixed and stained with terminal deoxynucleotidyl transferase dUTP nick end labeling (TUNEL) by using an ApopTag In Situ Apoptosis detection kit (S7111; Chemicon) and counterstained with DAPI, as per manufacturer's protocol. Fluorescent apoptotic cells were visualized using fluorescein excitation and emission filters.

Cytokine Analysis

Plasma cytokine detection and quantification was done at the Yale CytoPlex-multiplex core facility using the Multiplex System that analyzes 23 mouse cytokines.

Statistical Analyses

All in vivo studies included at least seven mice per genotype. For rescue studies using i.p. Wnt3a, n = 7 mice per group were used. All in vitro studies were carried out in three independent experiments in triplicate. Fluorescence and area measurements were done using Image J software (NIH). Preparation of graphs and all statistical analyses were carried out using GraphPad Prism 6 Project software (GraphPad). $p < 0.05$ was considered significant. Data are presented as mean ± SD.

SUPPLEMENTAL INFORMATION

Supplemental Information includes four figures and can be found with this article online at http://dx.doi.org/10.1016/j.celrep.2015.09.028.

ACKNOWLEDGMENTS

The authors gratefully acknowledge Dr. Kathleen Martin for reading the manuscript and providing valuable comments. The study was supported by NIH grant 1R01HL122830 and 1R01HL122822 (to A.M.).

Received: June 19, 2015
Revised: August 19, 2015
Accepted: September 10, 2015
Published: October 15, 2015

REFERENCES

Ait-Oufella, H., Taleb, S., Mallat, Z., and Tedgui, A. (2011). Recent advances on the role of cytokines in atherosclerosis. Arterioscler. Thromb. Vasc. Biol. *31*, 969–979.

Allahverdian, S., Chehroudi, A.C., McManus, B.M., Abraham, T., and Francis, G.A. (2014). Contribution of intimal smooth muscle cells to cholesterol accumulation and macrophage-like cells in human atherosclerosis. Circulation *129*, 1551–1559.

Cheng, Z., Biechele, T., Wei, Z., Morrone, S., Moon, R.T., Wang, L., and Xu, W. (2011). Crystal structures of the extracellular domain of LRP6 and its complex with DKK1. Nat. Struct. Mol. Biol. *18*, 1204–1210.

Cheng, S.L., Ramachandran, B., Behrmann, A., Shao, J.S., Mead, M., Smith, C., Krchma, K., Bello Arredondo, Y., Kovacs, A., Kapoor, K., et al. (2015). Vascular smooth muscle LRP6 limits arteriosclerotic calcification in diabetic LDLR-/- mice by restraining noncanonical Wnt signals. Circ. Res. *117*, 142–156.

Deniaud, E., Baguet, J., Chalard, R., Blanquier, B., Brinza, L., Meunier, J., Michallet, M.C., Laugraud, A., Ah-Soon, C., Wierinckx, A., et al. (2009). Overexpression of transcription factor Sp1 leads to gene expression perturbations and cell cycle inhibition. PLoS ONE *4*, e7035.

Dienz, O., and Rincon, M. (2009). The effects of IL-6 on CD4 T cell responses. Clin. Immunol. *130*, 27–33.

Farb, A., Burke, A.P., Tang, A.L., Liang, T.Y., Mannan, P., Smialek, J., and Virmani, R. (1996). Coronary plaque erosion without rupture into a lipid core. A frequent cause of coronary thrombosis in sudden coronary death. Circulation *93*, 1354–1363.

Feil, S., Fehrenbacher, B., Lukowski, R., Essmann, F., Schulze-Osthoff, K., Schaller, M., and Feil, R. (2014). Transdifferentiation of vascular smooth muscle cells to macrophage-like cells during atherogenesis. Circ. Res. *115*, 662–667.

Giannetti, M., Schroeder, H.A., Zalewski, A., Gonsalves, N., and Bryce, P.J. (2014). Dysregulation of the Wnt pathway in adult eosinophilic esophagitis. Dis. Esophagus, Published online August 28, 2014. http://dx.doi.org/10.1111/dote.12273.

Go, G.W., Srivastava, R., Hernandez-Ono, A., Gang, G., Smith, S.B., Booth, C.J., Ginsberg, H.N., and Mani, A. (2014). The combined hyperlipidemia caused by impaired Wnt-LRP6 signaling is reversed by Wnt3a rescue. Cell Metab. *19*, 209–220.

Gomez, D., and Owens, G.K. (2012). Smooth muscle cell phenotypic switching in atherosclerosis. Cardiovasc. Res. *95*, 156–164.

Gustavson, M.D., Crawford, H.C., Fingleton, B., and Matrisian, L.M. (2004). Tcf binding sequence and position determines beta-catenin and Lef-1 responsiveness of MMP-7 promoters. Mol. Carcinog. *41*, 125–139.

Hatzis, P., van der Flier, L.G., van Driel, M.A., Guryev, V., Nielsen, F., Denissov, S., Nijman, I.J., Koster, J., Santo, E.E., Welboren, W., et al. (2008). Genome-wide pattern of TCF7L2/TCF4 chromatin occupancy in colorectal cancer cells. Mol. Cell. Biol. *28*, 2732–2744.

Ishitani, T., Ninomiya-Tsuji, J., Nagai, S., Nishita, M., Meneghini, M., Barker, N., Waterman, M., Bowerman, B., Clevers, H., Shibuya, H., and Matsumoto, K. (1999). The TAK1-NLK-MAPK-related pathway antagonizes signalling between beta-catenin and transcription factor TCF. Nature *399*, 798–802.

Ishitani, T., Ninomiya-Tsuji, J., and Matsumoto, K. (2003). Regulation of lymphoid enhancer factor 1/T-cell factor by mitogen-activated protein kinase-related Nemo-like kinase-dependent phosphorylation in Wnt/beta-catenin signaling. Mol. Cell. Biol. *23*, 1379–1389.

Lin, X., Wang, Z., Gu, L., and Deuel, T.F. (1992). Functional analysis of the human platelet-derived growth factor A-chain promoter region. J. Biol. Chem. *267*, 25614–25619.

Mani, A., Radhakrishnan, J., Wang, H., Mani, A., Mani, M.A., Nelson-Williams, C., Carew, K.S., Mane, S., Najmabadi, H., Wu, D., and Lifton, R.P. (2007). LRP6 mutation in a family with early coronary disease and metabolic risk factors. Science *315*, 1278–1282.

Milewicz, D.M., Kwartler, C.S., Papke, C.L., Regalado, E.S., Cao, J., and Reid, A.J. (2010). Genetic variants promoting smooth muscle cell proliferation can result in diffuse and diverse vascular diseases: evidence for a hyperplastic vasculomyopathy. Genet. Med. *12*, 196–203.

Mill, C., and George, S.J. (2012). Wnt signalling in smooth muscle cells and its role in cardiovascular disorders. Cardiovasc. Res. *95*, 233–240.

Muendlein, A., Saely, C.H., Geller-Rhomberg, S., Sonderegger, G., Rein, P., Winder, T., Beer, S., Vonbank, A., and Drexel, H. (2011). Single nucleotide polymorphisms of TCF7L2 are linked to diabetic coronary atherosclerosis. PLoS ONE *6*, e17978.

Nalesso, G., Sherwood, J., Bertrand, J., Pap, T., Ramachandran, M., De Bari, C., Pitzalis, C., and Dell'accio, F. (2011). WNT-3A modulates articular chondrocyte phenotype by activating both canonical and noncanonical pathways. J. Cell Biol. *193*, 551–564.

Nusse, R. (2012). Wnt signaling. Cold Spring Harb. Perspect. Biol. *4*, pii: a011163.

Park, G.H., Plummer, H.K., 3rd, and Krystal, G.W. (1998). Selective Sp1 binding is critical for maximal activity of the human c-kit promoter. Blood *92*, 4138–4149.

Pereira, C.P., Bachli, E.B., and Schoedon, G. (2009). The wnt pathway: a macrophage effector molecule that triggers inflammation. Curr. Atheroscler. Rep. *11*, 236–242.

Ray, J.L., Leach, R., Herbert, J.M., and Benson, M. (2001). Isolation of vascular smooth muscle cells from a single murine aorta. Methods Cell Sci. *23*, 185–188.

Ross, R., and Glomset, J.A. (1973). Atherosclerosis and the arterial smooth muscle cell: Proliferation of smooth muscle is a key event in the genesis of the lesions of atherosclerosis. Science *180*, 1332–1339.

Schwartz, S.M., deBlois, D., and O'Brien, E.R. (1995). The intima. Soil for atherosclerosis and restenosis. Circ. Res. *77*, 445–465.

Shankman, L.S., Gomez, D., Cherepanova, O.A., Salmon, M., Alencar, G.F., Haskins, R.M., Swiatlowska, P., Newman, A.A., Greene, E.S., Straub, A.C., et al. (2015). KLF4-dependent phenotypic modulation of smooth muscle cells has a key role in atherosclerotic plaque pathogenesis. Nat. Med. *21*, 628–637.

Shen, S., Klamer, G., Xu, N., O'Brien, T.A., and Dolnikov, A. (2013). GSK-3β inhibition preserves naive T cell phenotype in bone marrow reconstituted mice. Exp. Hematol. *41*, 1016–27.e1.

Singh, R., De Aguiar, R.B., Naik, S., Mani, S., Ostadsharif, K., Wencker, D., Sotoudeh, M., Malekzadeh, R., Sherwin, R.S., and Mani, A. (2013a). LRP6 enhances glucose metabolism by promoting TCF7L2-dependent insulin receptor expression and IGF receptor stabilization in humans. Cell Metab. *17*, 197–209.

Singh, R., Smith, E., Fathzadeh, M., Liu, W., Go, G.W., Subrahmanyan, L., Faramarzi, S., McKenna, W., and Mani, A. (2013b). Rare nonconservative LRP6 mutations are associated with metabolic syndrome. Hum. Mutat. *34*, 1221–1225.

Sousa, A.G., Selvatici, L., Krieger, J.E., and Pereira, A.C. (2011). Association between genetics of diabetes, coronary artery disease, and macrovascular complications: exploring a common ground hypothesis. Rev. Diabet. Stud. *8*, 230–244.

Tan, N.Y., and Khachigian, L.M. (2009). Sp1 phosphorylation and its regulation of gene transcription. Mol. Cell. Biol. *29*, 2483–2488.

van Loosdregt, J., Fleskens, V., Tiemessen, M.M., Mokry, M., van Boxtel, R., Meerding, J., Pals, C.E., Kurek, D., Baert, M.R., Delemarre, E.M., et al. (2013). Canonical Wnt signaling negatively modulates regulatory T cell function. Immunity *39*, 298–310.

Virmani, R., Kolodgie, F.D., Burke, A.P., Farb, A., and Schwartz, S.M. (2000). Lessons from sudden coronary death: a comprehensive morphological classification scheme for atherosclerotic lesions. Arterioscler. Thromb. Vasc. Biol. *20*, 1262–1275.

Wang, H., Zhang, W., Tang, R., Hebbel, R.P., Kowalska, M.A., Zhang, C., Marth, J.D., Fukuda, M., Zhu, C., and Huo, Y. (2009). Core2 1-6-N-glucosaminyltransferase-I deficiency protects injured arteries from neointima formation in ApoE-deficient mice. Arterioscler. Thromb. Vasc. Biol. *29*, 1053–1059.

Wang, H., Liu, Q.J., Chen, M.Z., Li, L., Zhang, K., Cheng, G.H., Ma, L., and Gong, Y.Q. (2012). Association of common polymorphisms in the LRP6 gene with sporadic coronary artery disease in a Chinese population. Chin. Med. J. (Engl.) *125*, 444–449.

Wang, S., Song, K., Srivastava, R., Dong, C., Go, G.-W., Li, N., Iwakiri, Y., and Mani, A. (2015). Nonalcoholic fatty liver disease induced by noncanonical Wnt and its rescue by Wnt3a. FASEB J. *29*, 3436–3445. http://dx.doi.org/10.1096/fj.15-271171.

Xu, Y., Gong, W., Peng, J., Wang, H., Huang, J., Ding, H., and Wang, D.W. (2014). Functional analysis LRP6 novel mutations in patients with coronary artery disease. PLoS ONE *9*, e84345.

Zhang, X., Diab, I.H., and Zehner, Z.E. (2003). ZBP-89 represses vimentin gene transcription by interacting with the transcriptional activator, Sp1. Nucleic Acids Res. *31*, 2900–2914.